**Centerline Mach Number**

From total and static pressure measurements the centerline Mach numbers were calculated and plotted in Fig. 4 for $P_i = P_0 = 5$ ata. A normal shock is seen in the diverging section of the inner nozzle. Flow downstream of this shock is subsonic. Mach number decreases further up to about 20 mm from the nozzle exit. Farther downstream the flow accelerates up to the nozzle exit and beyond; perhaps due to flow separation in the diverging inner duct because of adverse pressure gradient and due to the presence of the outer flow impinging the inner flow at an angle. Superimposed on the axial Mach number distribution is a typical variation of centerline Mach number for a single, underexpanded, sonic jet. Figure 4 shows that the outer flow brings about a compression of the inner flow, creating a high static pressure zone near the exit of the inner nozzle similar to that of a highly underexpanded single flow. Injection angle of the outer flow may have a strong influence on the inner flow compression.

## Conclusions

Conclusions that may be drawn from this limited experimental study are the following. 1) It is possible to obtain a sizable Mach disk ($D_m \sim D_i$) using a relatively low pressure test facility by employing dual, coaxial, axisymmetric jets; brought about by compression of the inner flow in the near zone by the outer flow. 2) With such an arrangement the Mach disk size varies linearly with $P_i$, whereas $D_m/D_i$ variation with $P_0$ exhibits a maximum near $P_i = P_0$. 3) It is recognized that injection angle of the outer flow with respect to the inner may have a vital role in the Mach disk formation process. However, no tests were done varying the injection angle since the authors were primarily concerned with the study of the process of mixing of two coaxial high speed streams and not on the Mach disk formation process as such.

## References

[1]Eastman, D. W., and Radtke, C. P., "Location of the Normal Shock Wave in the Exhaust Plume of a Jet," *AIAA Journal*, Vol. 1, No. 4, 1963, pp. 918, 919.

[2]Crist, S., Sherman, P. M., and Glass, D. R., "Study of the Highly Underexpanded Sonic Jet," *AIAA Journal*, Vol. 4, No. 1, 1966, pp. 68–71.

[3]Abbett, M., "The Mach Disk in Underexpanded Exhaust Plumes," *AIAA Journal*, Vol. 9, No. 3, 1971, pp. 512–514.

[4]Lewis, C. H., and Carlson, D. J., "Normal Shock Location in Underexpanded Gas and Gas-Particle Jets," *AIAA Journal*, Vol. 2, No. 4, 1964, pp. 776, 777.

[5]Bauer, A. B., "Normal Shock Location of Underexpanded Gas-Particle Jets," *AIAA Journal*, Vol. 3, No. 6, 1965, pp. 1187–1189.

[6]Zukoski, E. E., and Spaid, F. W., "Secondary Injection of Gases into a Supersonic Flow," *AIAA Journal*, Vol. 2, No. 10, 1964, pp. 1689–1696.

[7]Schetz, J. A., and Billig, F. S., "Penetration of Gaseous Jets Injected into a Supersonic Stream," *Journal of Spacecraft and Rockets*, Vol. 3, No. 11, 1966, pp. 1658–1665.

# Front Body Effects on Drag and Flowfield of a Three-Dimensional Noncircular Cylinder

Khalid M. Sowoud* and E. Rathakrishnan†
*Indian Institute of Technology, Kanpur 208 016, India*

## Introduction

THE subject of drag reduction is an interesting practical problem with a wide range of applications. Because of the difficulties associated with theoretical analysis, the study of drag reduction has been almost entirely experimental. At high enough Reynolds numbers the flow past a bluff body is characterized by a large wake zone. The separated shear layers from the sharp corners feed vorticity to the wake. These vorticies are shed continuously downstream. The side faces and the rear face are subjected to low pressure, whereas the front face is subjected to high positive pressure. With this flow pattern, the pressure drag coefficient assumes very large values (1.0–1.42). This fact is particularly true for bluff bodies with noncircular cross-sections and sharp corners.[5]

Several investigations deal with drag reduction of bluff bodies. Some of them directly relevant to the present study are Refs. 2–9.

In the present study the shielding effect of square-plate and D-shaped front bodies on the drag reduction and the pressure distribution of a three-dimensional bluff body is investigated.

## Experimental Arrangement

The experiments were carried out in a $5.5 \times 3 \times 2$ ft low-speed, closed-circuit wind tunnel having a velocity range up to 45 m/s. The experimental model (Fig. 1) had three major parts. The rear body is a square box with windward sharp corners and rounded back with width $b_2 = 100$ mm, 108 mm long, and $R = 50$ mm. For the front body two shapes were used. The width of each front body varied from 0.25 to $1.0b_2$, and 12 different widths were tested. The gap between the front and rear bodies varied from 0.25 to $2.25b_2$, in steps of 0.25. The experiments were done for three speeds, which resulted in $Re_{b_2} = 1.0$, 1.4, and $1.8 \times 10^5$.

The drag force was measured directly using a three-component balance. For wall static pressure measurements the model was provided with 39 pressure taps, as shown in Fig. 1 (Sec. AA).

No blockage correction was done, since the configuration changes were not large, and all tests were made at zero angle of attack. At all runs, the blockage was only 1.79%.

## Results and Discussion

For the basic body, the measured drag coefficients $C_{D0}$ at the test Reynolds numbers based on rear-body width $b_2$ of 1.8, 1.4, and $1.0 \times 10^5$ were 1.42, 1.39, and 1.28, respectively. The high $C_{D0}$ is mainly due to the positive pressure at the front face and the low pressure at the rear surface, as seen from Fig. 2. Of course, the skin friction also will contribute to the drag,

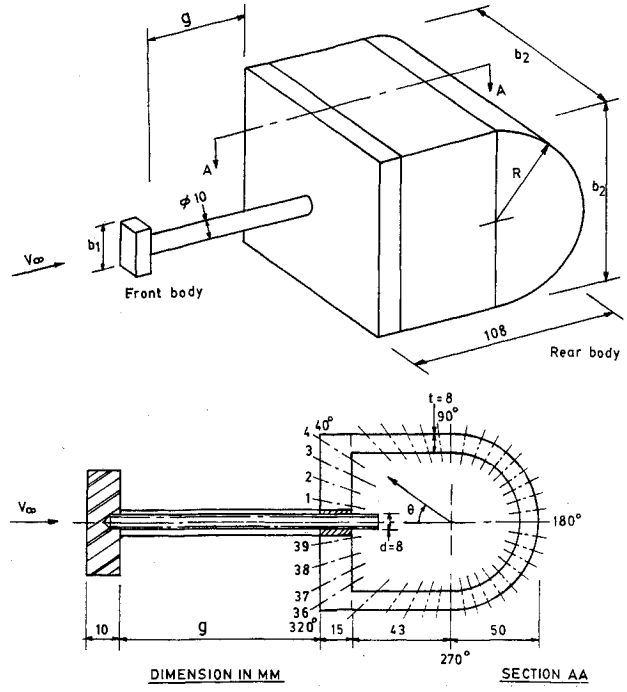


**Fig. 1 Schematic diagram of the experimental model; in Sec. AA the numbers 1–39 refer to pressure tap locations.**

Received March 9, 1992; revision received Oct. 12, 1992; accepted for publication Oct. 20, 1992. 

*Graduate Student, Department of Aerospace Engineering.
†Associate Professor, Department of Aerospace Engineering.

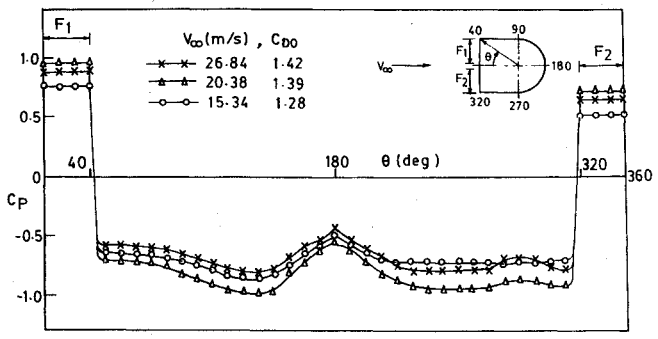


**Fig. 2 Pressure distribution for basic model.**

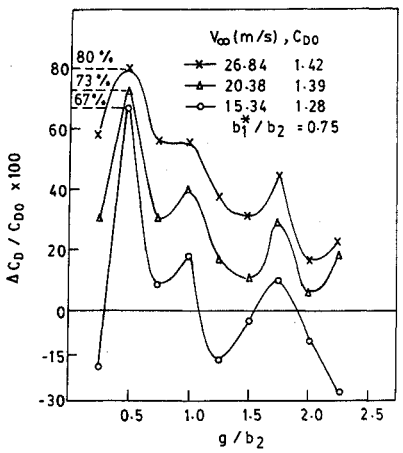


**Fig. 3 Percentage drag reduction for square-plate front body.**

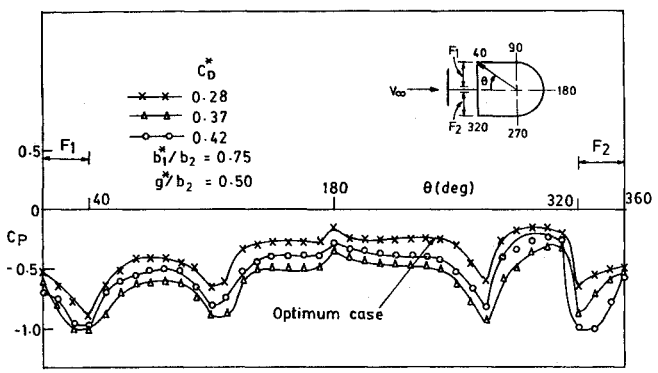


**Fig. 4 Pressure distribution on rear body surface midplane with square-plate front body.**

although the contribution of skin friction on bluff-body drag is small at these speeds.

### Drag Coefficient with Square-Plate Front Body

The drag reductions obtained for optimum combinations are shown in Fig. 3. The pressure distributions on the rear body for these runs are given in Fig. 4. From these figures, it is seen that the optimum combinations occurred at $g^*/b_2 = 0.50$, resulting in $C_D^*$ of 0.42, 0.37, and 0.28 at $Re = 1.0$, 1.4, and $1.8 \times 10^5$, respectively. These $C_D^*$ were 67, 73, and 80% below the $C_{D0}$. The maximum drag reduction of 80% was for the model with $b_1^*/b_2 = 0.75$ and $g^*/b_2 = 0.50$ as shown in Fig. 3. For this case the $C_P$ is negative everywhere on the face of the rear body as seen from Fig. 4. Further, it is heartening to note that at the gap ratio 0.50, $C_P$ at the front face of the model assumes values that are appreciably lower than those at the back.

The other tested geometries—$b_1/b_2 = 1.0$, 0.5, and 2.5—resulted in drag reductions in the range of 20–50%, which are quite low compared with the reduction at optimum (*) conditions.

**Table 1 Optimum drag regimes**

| Regime $C_D^*$ | I, Low | II, Medium | III, High |
|---|---|---|---|
| Optimum drag regimes for the combination with square-plate front body | | | |
| $Re = 1.0 \times 10^5$ | $<0.81$ | $0.81 < C_D^* < 0.98$ | $0.98 < C_D^* < 1.15$ |
| $Re = 1.4 \times 10^5$ | $<0.76$ | $0.76 < C_D^* < 0.84$ | $0.84 < C_D^* < 0.97$ |
| $Re = 1.8 \times 10^5$ | $<0.52$ | $0.52 < C_D^* < 0.72$ | $0.72 < C_D^* < 0.78$ |
| $b_1^*/b_2$ | 0.37–0.75 | 0.37–0.50 | 0.50–0.75 |
| $g^*/b_2$ | 0.25–0.75 | 0.75–1.50 | 1.50–2.25 |
| Optimum drag regimes for the combination with D-shaped front body | | | |
| $Re = 1.0 \times 10^5$ | $<0.42$ | $0.42 < C_D^* < 1.06$ | $1.06 < C_D^* < 1.13$ |
| $Re = 1.4 \times 10^5$ | $<0.62$ | $0.62 < C_D^* < 0.73$ | $0.73 < C_D^* < 1.00$ |
| $Re = 1.8 \times 10^5$ | $<0.46$ | $0.46 < C_D^* < 0.72$ | $0.72 < C_D^* < 0.88$ |
| $b_1^*/b_2$ | 0.25–0.75 | 0.25–0.625 | 0.25–0.625 |
| $g^*/b_2$ | 0.25–0.75 | 0.75–1.50 | 1.50–2.25 |

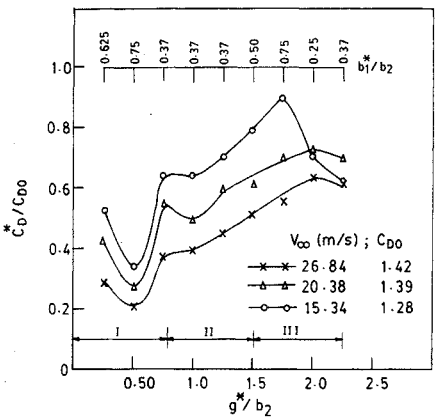


**Fig. 5 Minimum drag coefficient for each square plate and the gap at which it occurs; I, II, and III refer to flow regimes.**

### Drag Coefficient with D-Shaped Front Body

The optimum drag reduction obtained with a D-shaped front body was very much lower than that achieved with a square-plate front body. The maximum reduction in drag is only 70% as against the maximum reduction of 80% attained with a square-plate front body.

The total drag on the bluff-body combinations in the present study may be split into two parts: 1) one acting on the front body plus the front surface of the rear body and 2) the second being due to the base pressure on the rear body's rear surface.

The shear layers that separate from the front body interact with the rear body. At the optimum combination ($b_1^*/b_2$ and $g^*/b_2$), the rear body is fully submerged in the separated shear layers from the edges of the front body. Hence the entire face of the rear body is subjected to suction pressure. Therefore, the drag coefficient $C_D^*$ is very small compared with the $C_{D0}$. As the distance between the bodies increased ($g/b_2 > g^*/b_2$), the shear layers that separated from the front body attach onto the front face of the rear body, and there will be an alteration of the $C_P$ on the front face of the rear body. For this case the drag coefficient is more than $C_D^*$ but less than $C_{D0}$.

### Drag Regimes Based on Optimum Flow

Figure 5 gives $C_D^*$ variation with $g^*/b_2$, at different $b_1^*/b_2$. The optimum drag values measured are presented in Table 1. This classification of the optimum drag coefficient $C_D^*$ corresponds to distinctly different types of flow. The front body makes the streamlines that separate from its edges to attach

smoothly onto the front face shoulders of the main body, thereby converting the bluff body into an equivalent streamlined body to result in low drag. The drag touches the minimum at the optimum conditions.

## Conclusions

The experiments with two bluff bodies placed in tandem showed an impressive drag reduction at optimum conditions. The square-plate front body resulted in a maximum of 80% drag reduction. The D-shaped front body was less effective in reducing the drag compared with the square-plate front body.

## References

[1]Hoerner, S. F., *Fluid Dynamic Drag,* NJ, 1965.

[2]Morel, T., and Bohn, M., "Flow over Two Circular Disks In Tandem," *Transactions of the American Society of Mechanical Engineers, Journal of Fluids Engineering,* Vol. 102, March 1980, pp. 104–111.

[3]Koenig, K., and Roshko, A., "An Experimental Study of Geometrical Effects on the Drag and Flow Field of Two Bluff Bodies Separated by a Gap," *Journal of Fluid Mechanics,* Vol. 156, July 1985, pp. 167–204.

[4]Pamadi, B. N., Pereira, C., and Gowda, B. H. L., "Drag Reduction by Strakes of Noncircular Cylinders," *AIAA Journal,* Vol. 26, No. 3, 1986, pp. 292–299.

[5]Castro, I. P., and Robins, A. G., "The Flow Field Around a Surface Mounted Cube in Uniform and Turbulent Stream," *Journal of Fluid Mechanics,* Vol. 79, Pt. 2, 1977, pp. 307–335.

[6]Ogava, Y., and Oikava, S., "A Field Investigation of the Flow and Diffusion Around a Model Cube," *Atmospheric Environment,* Vol. 16, No. 2, 1982, pp. 207–222.

[7]Gowda, B. H. L., Gerhardt, H. J., and Kramer, C., "Surface Flow Field Around Three-dimensional Bluff Bodies," *Journal of Wind Engineering and Industrial Aerodynamics,* Vol. 11, 1983, pp. 405–420.

[8]Khalid, M., Palaniappan, C. T., and Rathakrishnan, E., "Passive Device for Base Drag Reduction," *Proceedings of the 18th National Conference on Fluid Mechanics and Fluid Power,* Indone, India, 1991, pp. G25–G34.

[9]Gowda, B. H. L., and Sitheeq, M., "Effect of Interference on the Pressure Distribution on a Three-Dimensional Bluff Body in Tandem Arrangement," *Indian Journal of Technology,* Vol. 29, No. 1, 1991, pp. 1–8.

# Subsonic/Transonic Cascade Flutter Using a Full-Potential Solver

Milind A. Bakhle,* T. S. R. Reddy,* and Theo G. Keith Jr.†
*University of Toledo, Toledo, Ohio 43606*

## Introduction

AEROELASTIC stability in transonic flow has received considerable attention in recent years. It has been observed[1,2] that the flutter speed of swept wings undergoes a sharp drop in the transonic regime; this has been referred to as the transonic flutter dip. This phenomenon is not modeled by the classical linear (flat-plate) aerodynamic theory. Hence, many nonlinear analyses have been used to model transonic flutter. However, all of the transonic flutter dip studies have been restricted to isolated airfoils. The blade-to-blade interaction in cascades, which is generally believed to be destabilizing, has not been considered in these analyses.

In the present work, the nonlinear unsteady full-potential aerodynamic solver of Refs. 3 and 4 is used for cascade flutter calculations in subsonic/transonic flow. Although the solver is nonlinear, the amplitude of blade motions is restricted to small values in the actual calculations. This ensures that the unsteady results are in the linear range (linear in the amplitude of motion); this allows efficient linear analysis methods to be used in the calculations. It should be noted that the steady flowfield is nonlinear and may be mixed subsonic/supersonic with shocks. In the present work, a frequency-domain analysis is used to calculate the flutter boundary for a cascade of NACA 64A010 airfoils; this airfoil section has been studied extensively in isolated airfoil transonic flutter studies. A comparison is made between the flutter results for a cascade and an isolated airfoil.

Presented as Paper 92-2119 at the AIAA Dynamics Specialist Conference, April 16–17, 1992; received April 24, 1992; revision received Nov. 21, 1992; accepted for publication Dec. 30, 1992. 

*Senior Research Associate, Department of Mechanical Engineering. Member AIAA.

†Distinguished University Professor, Department of Mechanical Engineering. Associate Fellow AIAA.

## Analysis

The aeroelastic model used in the present flutter analysis consists of a typical section structural model and an aerodynamic model based on the two-dimensional full-potential equation. Each blade of a bladed disk is represented by a rigid typical section model with two degrees of freedom—plunging and pitching. The aerodynamic model is based on the unsteady, two-dimensional, full-potential equation. The governing equation for irrotational, isentropic flow written in conservative form is

$$\frac{\partial \rho}{\partial t} + \frac{\partial (\rho u)}{\partial x} + \frac{\partial (\rho v)}{\partial y} = 0 \tag{1}$$

where

$$u = \frac{\partial \phi}{\partial x}, \qquad v = \frac{\partial \phi}{\partial y}$$

and

$$\frac{\rho}{\rho_\infty} = \left\{1 + \frac{(\gamma-1)}{2}\left[M_\infty^2 - \left(2\frac{\partial \phi}{\partial t} + [u^2+v^2]\right)\Big/ a_\infty^2\right]\right\}^{1/(\gamma-1)}$$

In the above, $\rho$ is the fluid (air) density, $u$ and $v$ the fluid velocity components in the $x$ and $y$ directions, $\phi$ the velocity potential, $a$ the sonic velocity, and $M$ the Mach number. The governing equation is transformed to the computational plane where it is discretized and solved using a finite volume scheme. The solution is obtained using a time-marching algorithm that uses approximate factorization at each time level with quasi-Newton iterations to maintain time accuracy. The method of solution is described in detail in Refs. 3 and 4.

For a frequency-domain flutter analysis, frequency-domain aerodynamic coefficients are required for plunging and pitching motions of specified frequency and specified interblade phase angle for a given cascade geometry and steady flow condition. These coefficients are calculated efficiently using the combined pulse response and influence coefficient method described in Ref. 5.

## Results and Discussion

### Unsteady Aerodynamics

To verify the calculation of frequency-domain aerodynamic coefficients in transonic flow, comparisons have been made between results from the present method and those from a linearized potential method[6]; these comparisons can be found in Ref. 7. In general, good agreement is seen between the corresponding results. However, significant differences are seen for the following calculation: an unstaggered cascade of single-circular-arc airfoils with a gap-to-chord ratio of 1.0, with a thickness-to-chord ratio of 0.05, and a steady flow Mach number of 0.76 at the far upstream and downstream locations. The reduced frequency of pitching is 1.0 based on the airfoil chord and the interblade phase angle is 180 deg.

Since the present calculations are restricted to small amplitude motions, the present analysis is comparable to the linearized potential calculations of Ref. 6. Any differences in the results must be attributed to differences in the numerical scheme, boundary conditions, and discretization. Efforts are underway to isolate and eliminate these differences. A comparison of the unsteady pressure distribution is shown in Fig. 1 to demonstrate that both results are qualitatively similar. These results were obtained using a $61\times31$ grid with 61 points in the streamwise direction and 31 points in the direction of the stagger line in each blade passages; 31 points are